Eur. Phys. J. Special Topics **226**, 1857–1866 (2017)

DOI: 10.1140/epjst/e2017-70023-1

THE EUROPEAN PHYSICAL JOURNAL SPECIAL TOPICS

Regular Article

Transition from complete synchronization to spatio-temporal chaos in coupled chaotic systems with nonhyperbolic and hyperbolic attractors

Elena Rybalova, Nadezhda Semenova, Galina Strelkova, and Vadim Anishchenko[a]

Saratov State University, 83 Astrakhanskaya street, Saratov, 410012, Russia

Received 30 January 2017 / Received in final form 9 March 2017
Published online 21 June 2017

Abstract. We study the transition from coherence (complete synchronization) to incoherence (spatio-temporal chaos) in ensembles of nonlocally coupled chaotic maps with nonhyperbolic and hyperbolic attractors. As basic models of a partial element we use the Henon map and the Lozi map. We show that the transition to incoherence in a ring of coupled Henon maps occurs through the appearance of phase and amplitude chimera states. An ensemble of coupled Lozi maps demonstrates the coherence-incoherence transition via solitary states and no chimera states are observed in this case.

1 Introduction

Exploring synchronization, different pattern formation in coupled nonlinear systems as well as studying their stability and evolution is one of the most important and rapidly developing topic of research in the nonlinear science and its applications. Recently a new form of dynamics called chimera state attracted a lot of attention [1–16]. These chimera states arise in networks of nonlocally coupled identical oscillators and consists of parts with spatially coherent (synchronous) dynamics and regions where spatial coherence is lost (desynchronous dynamics). Initially, this effect has been found in regular networks of nonlocally coupled identical phase oscillators in [1]. Later, this kind of dynamics was called "chimera state" [2] for its similarity to the mythological Greek beast made up of incongruous parts. In recent years the interest in studying chimera states has rapidly increased. It has been recently shown that chimera states can also arise in networks with different types of network elements ranging from discrete-time [3] and continuous-time [4] chaotic models, Van der Pol oscillators [5,6] to population models [7] and autonomous Boolean networks [8]. This effect has also been found experimentally in chemical reactions [9,10] and laser arrays [11,12]. Recently a number of works were published where a possible application of

[a] e-mail: wadim@info.sgu.ru

chimera states is studied to describe the dynamics of real-world ensembles and living systems [17–20].

It is quite interesting to explore how the properties of individual elements of an ensemble can influence the appearance of chimera states. The first attempt to generalize the already obtained results on ensembles of elements with chaotic dynamics has been made in [13]. The authors propose certain properties of partial elements, which are necessary for chimeras to appear in their ensembles. In particular, they hypothesize that chimera states can be realized only in ensembles of coupled systems with nonhyperbolic chaotic attractors. This hypothesis has been corroborated for nonhyperbolic systems such as the logistic map [3], the Henon map [13], the Rössler system [4], and the Anishchenko-Astakhov oscillator [15]. It has also been shown in [13] that chimera states cannot be found in ensembles of systems with singular hyperbolic attractors (for example, the Lozi map [13] and the Lorenz system [21]).

Based on the results in [13], in our research we employ the Henon map [22]

$$\begin{aligned} x^{t+1} &= 1 - \alpha(x^t)^2 + y^t, \\ y^{t+1} &= \beta x^t, \end{aligned} \tag{1}$$

and the Lozi map [23]

$$\begin{aligned} x^{t+1} &= 1 - \alpha|x^t| + y^t, \\ y^{t+1} &= \beta x^t, \end{aligned} \tag{2}$$

as basic models for partial elements in networks of nonlocally coupled chaotic systems with different types of chaotic attractors. In both maps given above, t is the discrete time ($t = 1, 2, \ldots$), α and β are control parameters.

The Henon map (1) describes the dynamics of a sufficiently wide class of chaotic systems. It can be transformed to the classical logistic map when $\beta \to 0$. Three-dimensional continuous-time systems with a chaotic attractor emerging in the neighborhood of a saddle-focus separatrix loop (Shilnikov's theorem [24]) are characterized by a map in a secant plane, which is topologically equivalent to the map (1) [25]. Therefore, we can suggest that the map (1) is a sufficiently general model of systems with a chaotic attractor which is formed through a cascade of period-doubling bifurcations, i.e., systems with a chaotic quasiattractor [26].

The Lozi map is especially introduced to describe the structure and properties of the Lorenz attractor, which is known to be a singular hyperbolic attractor in a bounded range of system parameter values. The Lozi map exhibits a singular hyperbolic attractor and is not characterized by multistability. This map (2) also describes the dynamics of a rather broad class of chaotic systems with hyperbolic and nearly hyperbolic attractors. When $\beta \to 0$, the map (2) transforms to a one-dimensional map of the hyperbolic type, the so-called tent map. The map (2) is topologically equivalent to a map in a secant plane of three-dimensional continuous-time systems with Lorenz-type attractors.

In the present paper we study coherence–incoherence transitions in ensembles of nonlocally coupled Henon and Lozi maps and describe their similarities and fundamental differences. We also show that these networks fully reproduce the basic effects, which have been obtained for ensembles of oscillators with nonhyperbolic and hyperbolic chaotic attractors. These findings enable one to substantiate the choice of maps (1) and (2) as basic models of chaotic systems.

2 Models under study

The first model, which we use to study in our paper, is a one-dimensional ensemble of nonlocally coupled Henon maps:

$$x_i^{t+1} = f_x(x_i^t, y_i^t) + \frac{\sigma_x}{2P} \sum_{j=i-P}^{i+P} [f_x(x_j^t, y_j^t) - f_x(x_i^t, y_i^t)],$$
$$y_i^{t+1} = f_y(x_i^t, y_i^t) + \frac{\sigma_y}{2P} \sum_{j=i-P}^{i+P} [f_y(x_j^t, y_j^t) - f_y(x_i^t, y_i^t)], \quad (3)$$

where t denotes the discrete time, $i = 1, 2, \ldots, N$ is the index of an oscillator, N is the number of all elements in the ring, σ_x and σ_y are the coupling coefficients, P denotes the number of nearest neighbors in each direction in the ring. Function $f_x(x, y)$ is specified by the first equation of the Henon map, $f_x(x, y) = 1 - \alpha x^2 + y$, and $f_y(x, y)$ is given by the second equation, $f_y(x, y) = \beta x$. We introduce the coupling radius $r = P/N$ and assume that $\sigma_x = \sigma$ and $\sigma_y = 0$. In this case we can rewrite the system (3) as follows:

$$x_i^{t+1} = f_x(x_i^t, y_i^t) + \frac{\sigma}{2P} \sum_{j=i-P}^{i+P} [f_x(x_j^t, y_j^t) - f_x(x_i^t, y_i^t)],$$
$$y_i^{t+1} = f_y(x_i^t, y_i^t). \quad (4)$$

With a little manipulation the system (4) can be represented in a different form:

$$x_i^{t+1} = (1 - \sigma) f_x(x_i^t, y_i^t) + \frac{\sigma}{2P} \sum_{j=i-P; j \neq i}^{i+P} f_x(x_j^t, y_j^t),$$
$$y_i^{t+1} = f_y(x_i^t, y_i^t). \quad (5)$$

The second term in (5) describes the effect of $2P$ neighbors only, i.e., it characterizes only nonlocal coupling. The first term in (5) illustrates transformations of the ith oscillator without coupling with $2P$ neighboring oscillators.

As follows from (5), σ is the main bifurcation parameter in the system (4). Varying its values we can control the dynamics of the first and second terms in (5). Hereinafter the parameters of the Henon map are fixed as $\alpha = 1.4$ and $\beta = 0.2$. These values yield a regime of fully developed chaos in an individual element of (5) without coupling. Two limit values of σ can be distinguished. When $\sigma \to 1$, the dynamics of (4) is described by the second term in (5) and the regime of complete chaotic synchronization is realized in the ensemble (4). When $\sigma \to 0$, we have an ensemble of uncoupled chaotic oscillators. If initial conditions are chosen to be random, the oscillators are completely desynchronized both in time and in space. For $0 < \sigma < 1$, the dynamics of (4) is defined by both terms in (5) and, as has been recently shown, phase and amplitude chimera states can be realized in this case [14,15].

Similarly, we introduce a network of coupled Lozi maps by using the system (5). Now the function $f_x(x, y)$ in (5) is given by the first equation of the Lozi map (2), $f_x(x, y) = 1 - \alpha|x| + y$, and $f_y(x, y)$ is specified by the second equation of (2), $f_y(x, y) = \beta x$. We fix the control parameters of the Lozi map at $\alpha = 1.4$ and $\beta = 0.3$. These values correspond to a chaotic regime with a positive value of the maximal Lyapunov exponent. Other parameters are the same as in (4) and (5).

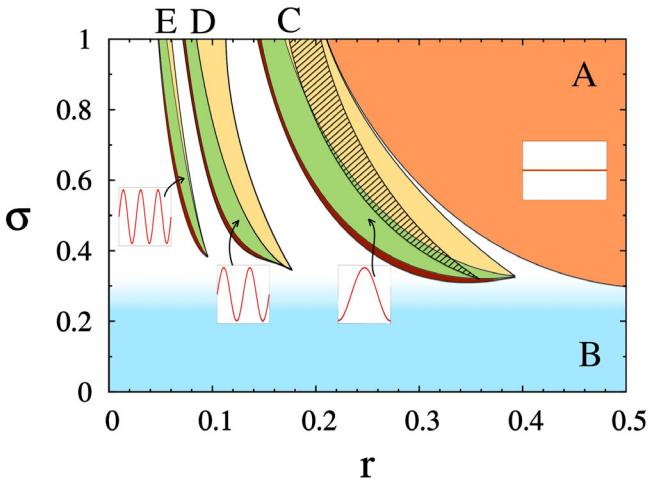

Fig. 1. Bifurcation diagram for the network of coupled Henon maps in the (r, σ) parameter plane. A denotes the region of complete chaotic synchronization, B is the region of complete incoherence. C, D, and E are the coherence regions with the wave numbers $k = 1, 2$, and 3, respectively. Inside these regions, the light gray tone (yellow color) marks period-2 temporal dynamics, gray tone (green) – period-4 dynamics, and dark gray tone (red) – period-8 dynamics. The hatched region corresponds to the coherence regimes shown in Figures 2e and 2f. The insets display snapshots of typical coherent states. System parameters: $\alpha = 1.4$, $\beta = 0.2$, and $N = 1000$.

As can be seen from (5), the second term in the first equation describes the effect of neighbors $i - P \le j \le i + P$ on the ith oscillator. We denote it as $\Phi_i^t = \frac{\sigma}{2P} \sum_{j=i-P; j\neq i}^{i+P} f_x(x_j^t, y_j^t)$ and call it *the coupling function*.

3 Transition from coherence to incoherence in the network of coupled Henon maps

We start our study by constructing a bifurcation diagram for the ensemble of coupled Henon maps, which is depicted in Figure 1 in the (r, σ) parameter plane. Region A corresponds to complete chaotic synchronization and B refers to the region of complete desynchronization. Letters C, D, and E denote the coherence regions with wave numbers $k = 1$, 2, and 3, respectively [3]. The corresponding coherent states x_i^t are shown as snapshots in the insets of Figure 1. In the context of temporal dynamics, subregions with period-2, 4, and 8 dynamics can be distiguished inside these regions.

For further investigations we fix the coupling radius at the value $r = 0.32$ and decrease the coupling strength σ from 1 to 0. At the beginning we consider the destruction of complete chaotic synchronization (Fig. 2). In order to analyze the peculiarities of the temporal dynamics we use the method proposed in [15]. For each partial element $1 \le i \le 1000$, we plot the last 50 iterations of x_i^t or Φ_i^t ($9950 \le t \le 10000$). This method enables one to diagnose the oscillation mode (periodic or chaotic) and to find the oscillation period and regimes of synchronization (desynchronization) in an ensemble. We call this graphical illustration as a "spatio-temporal profile". If necessary, we also plot instantaneous spatial profiles (snapshots) for a fixed discrete time $t = \text{const}$.

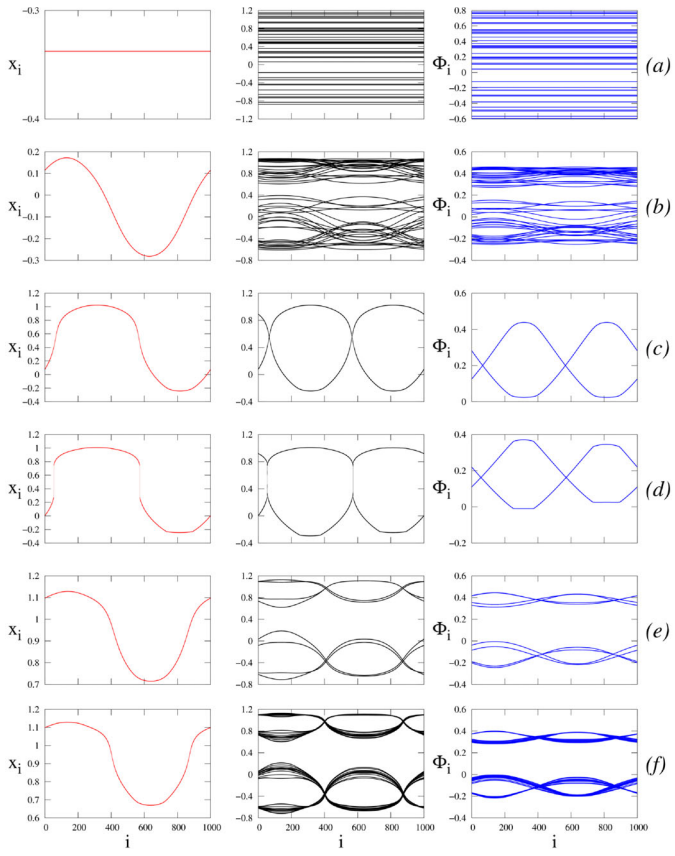

Fig. 2. Snapshots and spatio-temporal profiles of the dynamics of the network of coupled Henon maps for decreasing coupling strength σ. Left panels show snapshots at $t = 10000$, center panels correspond to the last 50 instantaneous spatial profiles of x_i^t, right panels depict the last 50 snapshots for the coupling function Φ_i^t. (a) Complete chaotic synchronization regime at $\sigma = 0.68$, (b) partial chaotic synchronization regime at $\sigma = 0.49$, (c) emergence of period-2 oscillations at $\sigma = 0.48$, (d) appearance of two breaks in the snapshot at $\sigma = 0.41$, (e) and (f) correspond to the network dynamics in the hatched region in Figure 1 at $\sigma = 0.408$ and $\sigma = 0.368$, respectively. Other parameters: $\alpha = 1.4$, $\beta = 0.2$, and $r = 0.32$.

When $\sigma \in A$ (for $r = 0.32$ this regime is realized when $0.48 < \sigma \leq 1.0$), the network of coupled Henon maps demonstrates the regime of complete chaotic synchronization both in space and in time (Fig. 2a). All the elements have the same values x_i at any time (Fig. 2a, left panel). The temporal evolution of x_i^t values is chaotic but synchronous for all the elements (Fig. 2a, center panel). A new interesting regime (Fig. 2b) can be observed between A and C regions (the white area in Fig. 1). The snapshot (Fig. 2b, left panel) differs from a straight line but is described by a smooth and slowly varying function. The neighboring elements have close x_i values, i.e., the following inequality holds:

$$|x_i^t - x_{i+1}^t| < \delta, \qquad \delta \ll 1. \tag{6}$$

The spatial profile (snapshot) oscillates irregularly (chaotically) in time (Fig. 2b, center panel) but still remains a smooth and slowly varying function. We call this regime as partial chaotic synchronization. In this case the neighboring oscillators

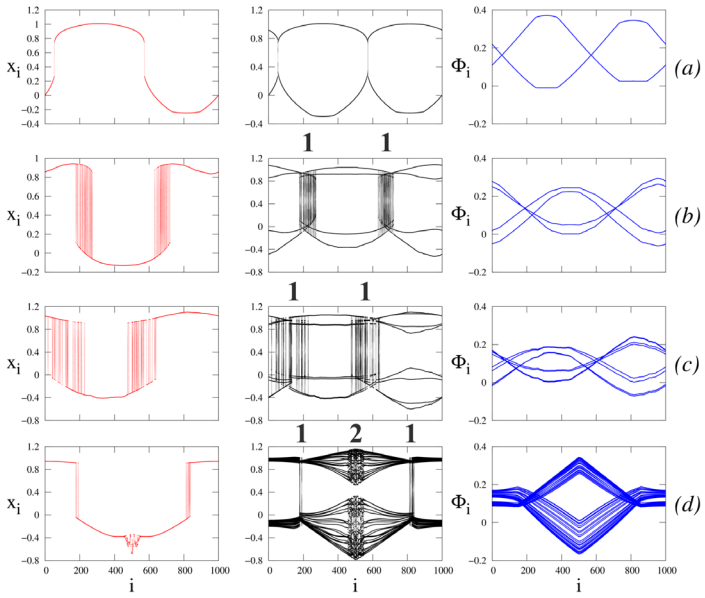

Fig. 3. Snapshots (left column) and spatio-temporal profiles (center column) of the dynamics of the network of coupled Henon maps, and spatio-temporal profiles for the coupling function Φ_i^t (right column) for different values of the coupling strength: (a) $\sigma = 0.41$, (b) $\sigma = 0.316$, (c) $\sigma = 0.26$, and (d) $\sigma = 0.258$. 1 marks the phase chimera regime, 2 denotes the amplitude chimera regime. Other parameters: $\alpha = 1.4$, $\beta = 0.2$, and $r = 0.32$.

behave almost synchronously but the synchronization degree is gradually destroyed when the distance between the oscillators increases.

When $\sigma \approx 0.48$, the ensemble demonstrates stable 2-periodic oscillations (Fig. 2c). The front of the wave-like profile (Fig. 2c, left panel) and the spatio-temporal profile (Fig. 2c, center panel) become steeper. This regime corresponds to the coherence domain C (light gray (yellow)) in the diagram in Figure 1. The coupling function also demonsrates the 2-periodic dynamics (Fig. 2c, right panel).

With a further decrease of the coupling strength σ the spatial profiles loose their smoothness and split into upper and lower branches. Many works state that this is one of the main reasons for the appearance of chimera states [3,4]. At the points where the spatial profile breaks up, the spatial derivative tends to infinity (Fig. 2d). The discontinuity of the wave-like profile is caused by drastic changes in the oscillation phase. The oscillations of the elements from the upper and lower branches in the profiles (Fig. 2d (left and center panels)) are 2-periodic but they are shifted in phase by a half-period with respect to each other.

As can be seen from Figure 1, the hatched region, that corresponds to the regime shown in Figures 2e and 2f, is superimposed on the coherence region C. The spatial profiles are still coherent but the temporal dynamics differs from the regimes depicted in Figures 2c and 2d. The superposition of two domains in Figure 1 means that we can observe either the regime in Figures 2c and 2d or the regime shown in Figures 2e and 2f by changing initial conditions.

Further decreasing σ leads to the birth of a phase chimera state [4,15] in the neighborhood of the profile breaks (Fig. 3a). This regime is characterized by period-4 oscillations. The oscillators from the coherence cluster have equal phases unlike the oscillators from the incoherence region, which are shifted in phase by a half-period. The coupling function Φ_i^t also demonstrates 4-periodic oscillations. The regime

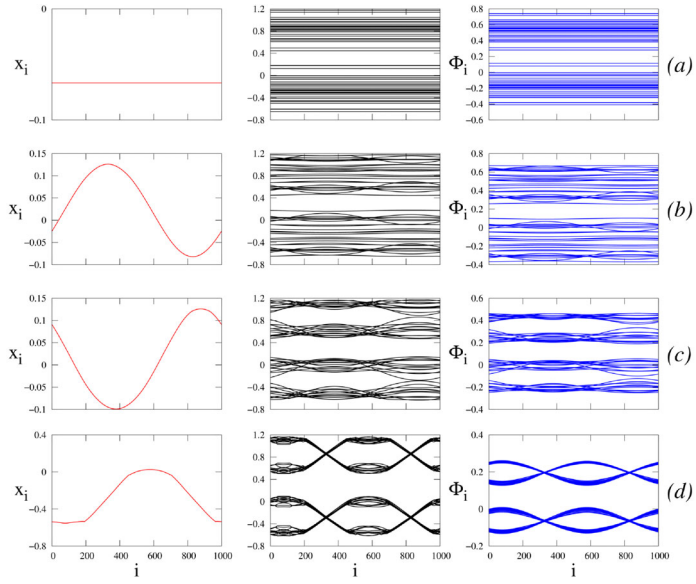

Fig. 4. Snapshots (left column) and spatio-temporal profiles (center column) for the dynamics of the network of coupled Lozi maps, and spatio-temporal profiles of the coupling functions Φ_i^t (right column) with decreasing coupling strength: (a) $\sigma = 0.63$, (b) $\sigma = 0.57$, (c) $\sigma = 0.4$, and (d) $\sigma = 0.23$. System parameters: $\alpha = 1.4$, $\beta = 0.3$, and $r = 0.193$.

described is shown in Figure 3b. It must be noted that the period-4 oscillatory regime can be realized without phase chimeras. This implies that the instantaneous spatial profile can be coherent and has two breaks like in Figure 3a. However, the temporal dynamics with oscillation period ≥ 4 is the basic condition for the chimera state appearance. When σ decreases further, a period doubling cascade takes place in time (Fig. 3c) and finally, the network dynamics becomes chaotic at $\sigma \approx 0.258$. This evolution process is accompanied by the appearance of an amplitude chimera which can either coexist with the phase chimera (Fig. 3d) or not. The amplitude chimera cluster occupies the network domain $450 \leq i \leq 550$, in which the elements behave chaotically and are desynchronized. When $\sigma \leq 0.25$, the network demonstrates the transition to spatio-temporal chaos (Fig. 1).

4 Coherence-incoherence transition in the ensemble of coupled Lozi maps

Our numerical studies of oscillation regimes for the network of coupled Lozi maps in the (r, σ) parameter plane have shown that only two regions can be clearly distinguished, namely, the region of complete chaotic synchronization and the region of spatio-temporal chaos. Regions with periodic oscillations, like regions C, D, and E in Figure 1, cannot be defined. However, in the ensemble of coupled Lozi maps, there are regions of travelling waves which highly depend on initial conditions.

In analogy to the ensemble of coupled Henon map, we explore the transition from complete synchronization to spatio-temporal chaos in the network of coupled Lozi maps by decreasing the coupling strength σ from 1 to 0 for a fixed value of the coupling radius $r = 0.193$. Numerical results are shown in Figures 4 and 5.

The regime of complete chaotic synchronization is realized in the ensemble of coupled Lozi maps within the range $0.62 < \sigma < 1.0$ (Fig. 4a). With a decrease of σ,

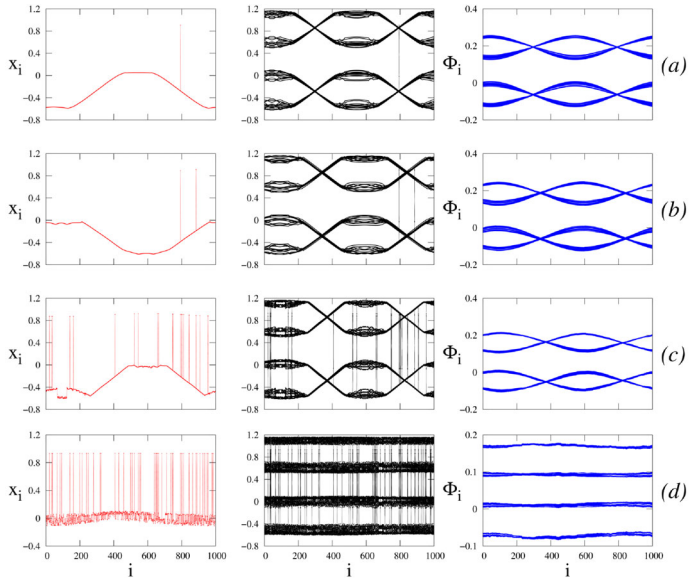

Fig. 5. Snapshots (left column) and spatio-temporal profiles (center column) of the dynamics of the network of coupled Lozi maps, and spatio-temporal profiles of Φ_i^t (right column) for different values of the coupling strength: (a) $\sigma = 0.226$, (b) $\sigma = 0.219$, (c) $\sigma = 0.193$, and (d) $\sigma = 0.165$. Other parameters: $\alpha = 1.4$, $\beta = 0.3$, and $r = 0.193$.

the temporally chaotic but spatially coherent dynamics is observed in the ensemble (Fig. 4b). For $\sigma \in [0.295; 0.48]$, the values of x_i^t states are divided and formed four separate domains (Fig. 4c). Then the distribution of the x_i values becomes less and for $\sigma \geq 0.227$ the network starts operating in a nearly regular 4-periodic mode (Fig. 4d). At the same time, the snapshots shown in Figures 4b–4d (left panels) illustrate coherent wave-like profiles.

As the coupling strength σ decreases further, the network of coupled Lozi maps can exhibit regimes which are not realized in the ring of coupled Henon maps. Several separate oscillators in the network of coupled Lozi maps demonstrate abrupt jumps in their amplitudes. Such regimes are called solitary states [16]. When $\sigma \approx 0.226$, there is only a single solitary state (Fig. 5a). The number of solitary states grows almost linearly as σ decreases (Figs. 5b–5d).

Thus, the transition to spatial incoherence (spatio-temporal chaos) in the ensemble of coupled Lozi maps occurs through a gradual growth of the number of solitary states. No chimera states are observed in this case.

5 Conclusions

We have studied the peculiarities of transitions from coherence to incoherence in ensembles of coupled chaotic maps with different types of a chaotic attractor. Comparative analysis of the numerical results obtained for the networks of coupled Henon maps and Lozi maps has shown that for large values of the coupling strength σ, the regime of complete chaotic synchronization can be realized in both systems. This is substantiated by the dominant role of the coupling function Φ_i^t in (5). The regime of spatio-temporal chaos (complete incoherence or desynchronization) is also observed in both ensembles. In this case, the prevailing role belongs rather to the local dynamics of individual elements in both ensembles (the first term in (5)) because the coupling

strength is sufficiently weak. However, there is a fundamental difference in the transition between these two regimes in the considered networks. When $0 < \sigma < 1$, the contribution of both the first and second terms in (5) appears to be significant. For the ensemble of coupled Henon maps, the transition to complete incoherence occurs through the appearance of phase and amplitude chimera states, while no chimeras are found in the ensemble of coupled Lozi maps. In the latter system, the dynamics evolves to spatio-temporal chaos via solitary states. We also note that the traveling wave regime can be observed in the network of coupled Lozi maps. This kind of dynamics has already been found in an ensemble of coupled Lorenz systems and has not been encountered in networks of coupled logistic maps, Henon maps and Rössler systems.

Thus, we can generalize the results summarized above. Ensembles of nonlocally coupled systems with a singular hyperbolic attractor (the Lozi map or the Lorenz-type systems) can demonstrate regimes of travelling waves and solitary states. These latter typically accompany the transition to spatio-temporal chaos in such networks. A different mechanism is exhibited by ensembles of nonlocally coupled systems with a nonhyperbolic attractor (e.g., the logistic map, the Henon map, the Rössler system). The transition from coherence to incoherence in those networks is realized through chimera states.

This work is supported in the framework of SFB910 and RFBR (Grant No. 15-02-02288).

References

1. Y. Kuramoto, D. Battogtokh, Nonlin. Phen. Complex Syst. **5**, 380 (2002)
2. D.M. Abrams, S.H. Strogatz, Phys. Rev. Lett. **93**, 174102 (2004)
3. I. Omelchenko, Y. Maistrenko, P. Hövel, E. Schöll, Phys. Rev. Lett. **106**, 234102 (2011)
4. I. Omelchenko, B. Riemenschneider, P. Hövel, Y. Maistrenko, E. Schöll, Phys. Rev. E **85**, 026212 (2012)
5. I. Omelchenko, A. Provata, J. Hizanidis, E. Schöll, P. Hövel, Phys. Rev. E **91**, 022917 (2015)
6. V. Bastidas, I. Omelchenko, A. Zakharova, E. Schöll, T. Brandes, Phys. Rev. E **92**, 062924 (2015)
7. J. Hizanidis, E. Panagakou, I. Omelchenko, E. Schöll, P. Hövel, A. Provata, Phys. Rev. E **92**, 012915 (2015)
8. D.P. Rosin, D. Rontani, D.J. Gauthier, Phys. Rev. E **89,** 042907 (2014)
9. V. Vanag, I. Epstein, Phys. Rev. Lett. **87**, 228301 (2001)
10. M.R. Tinsley, S. Nkomo, K. Showalter, Nat. Phys. **8**, 662 (2012)
11. F. Rogister, R. Roy, Phys. Rev. Lett. **98**, 104101 (2007)
12. F. Böhm, A. Zakharova, E. Schöll, K. Lüdge, Phys. Rev. E **91**, 040901(R) (2015)
13. N. Semenova, A. Zakharova, E. Schöll, V. Anishchenko, Europhys. Lett. **112**, 40002 (2015)
14. T.E. Vadivasova, G.I. Strelkova, S.A. Bogomolov, V.S. Anishchenko, Chaos **26**, 093108 (2016)
15. S.A. Bogomolov, A.V. Slepnev, G.I. Strelkova, E. Schöll, V.S. Anishchenko, Commun. Nonlin. Sci. Numer. Simulat. **43**, 25 (2017)
16. Yu. Maistrenko, B. Penkovsky, M. Rosenblum, Phys. Rev. E **89**, 060901 (2014)
17. R. Levy, W.D. Hutchison, A.M. Lozano, J.O. Dostrovsky, J. Neurosci. **20**, 7766 (2000)
18. N.C. Rattenborg, C.J. Amlaner, S.L. Lima, Neurosci. Biobehav. Rev. **24**, 817 (2000)
19. S. Funahashi, C.J. Bruce, P.S. Goldman-Rakic, J. Neurophysiol. **65**, 1464 (1991)
20. N.V. Swindale, Proc. R. Soc. London B: Biol. Sci. **208**, 243 (1980)
21. V. Dziubak, Y. Maistrenko, E. Schöll, Phys. Rev. E **87**, 032907 (2013)
22. M. Hénon, Comm. Math. Phys. **50**, 69 (1976)

23. R. Lozi, J. Phys. Colloques **39**, C5-9 (1978)
24. L.P. Shilnikov, Math. Sbornik **81**, 92 (1970) (in Russian)
25. V.S. Anishchenko, *Dynamical Chaos – Models and Experiments* (World Scientific, Singapore, 1995)
26. V.S. Afraimovich, L.P. Shilnikov, in *Nonlinear dynamics and turbulence*, edited by G. Barenblatt, G. Iooss, D.D. Joseph (Pitman, London, 1983) pp. 1–34